Wu, Z., Yin, Q., Guo, Z., & Berger, A. (2020). Hemisphere differences in response of sea surface temperature and sea ice to precession and obliquity. Global and Planetary Change, 192, 103223.

Hemisphere differences in response of sea surface temperature and sea ice to precession and obliquity

Zhipeng Wu[a,b,c], Qiuzhen Yin[a*], Zhengtang Guo[b,c,d], André Berger[a]

[a]Georges Lemaître Center for Earth and Climate Research, Earth and Life Institute, Université catholique de Louvain, Louvain-la-Neuve, Belgium

[b]Key Laboratory of Cenozoic Geology and Environment, Institute of Geology and Geophysics, Chinese Academy of Sciences, Beijing, China

[c]University of Chinese Academy of Sciences, Beijing, China

[d]CAS Center for Excellence in Life and Paleoenvironment, Beijing, China

*Corresponding author: Qiuzhen Yin (qiuzhen.yin@uclouvain.be)

Address: Université catholique de Louvain, Place Louis Pasteur, 3, L4.03.08, B-1348, Louvain-la-Neuve, Belgium.

Abstract

The response of the climate system to astronomical parameters is an important scientific issue, but the internal processes and feedbacks need to be better understood. This study investigates the differences of the climate response to the astronomical forcing between the Northern (NH) and Southern (SH) hemispheres based on a more than 90,000-year long transient simulation using the model LOVECLIM. The astronomical parameters of the period 511-417 ka BP covering MIS-13, MIS-12 and MIS-11 are used, and Greenhouse gas (GHG) concentrations and ice sheets are fixed, in order to investigate the role of insolation alone. Our results show that the response of sea ice and sea surface temperature (SST) to precession and obliquity is different between the two hemispheres. Precession plays a dominant role on the Arctic sea ice. This is mainly due to its response to the local summer insolation and also, to a less degree, the influence of the northward oceanic heat transports. However, obliquity plays a dominant role on the Southern Ocean sea ice through its influence on local solar radiation and also on the westerly winds. As far as the SST is concerned, it shows a strong precession signal at low latitudes in both hemispheres. For the SST in the mid and high latitudes, obliquity plays a dominant role in the SH whereas precession is more important in the NH. This is largely due to the different response to insolation and feedbacks related to the different land-ocean distribution in the two hemispheres. Near the Equator, besides the precessional signal, the SST also shows strong half-precessional signal, which can be explained by the unique characteristics of the insolation variations at the Equator. Our results also show that during the period of low eccentricity, obliquity is always more important than precession and the half-precessional signal vanishes due to reduced impact of precession, but precession is always more important in the NH than in the SH.

Keywords: Precession, Obliquity, Half-precession, Sea ice, Sea surface temperature, Northern Hemisphere, Southern Hemisphere, Paleoclimate modeling

1 Introduction

As one of the most important drivers of the climate system, the incoming solar radiation (insolation), depends largely on the three astronomical parameters: eccentricity, obliquity and climatic precession (Berger, 1976, 1978). The total energy received by the whole Earth over one year is only a function of eccentricity, while obliquity and precession can modify the latitudinal-seasonal distribution of insolation (Berger, 1988; Loutre et al., 2004; Berger et al., 2010). Astronomical theory of paleoclimate has been generally accepted and widely used in the research of paleoclimate, especially during the last 40 years (Hays et al., 1976), and the astronomical signals have been found in plenty of geological records like deep-sea sediments, continental archives and ice cores.

With the richness of the geological records, much attention has been paid on the relationship between different climatic variables and the astronomical parameters. For example, the relationship between SST and the astronomical parameters have been discussed based on marine records from the Pacific (eg. de Garidel-Thoron et al., 2005), Atlantic (eg. Lawrence et al., 2009) and Indian Ocean (eg. Howard and Prell, 1992). The response of other climatic variables to astronomical forcing have also been discussed, like sea ice (eg. Cronin et al., 2013), vegetation (eg. Joannin et al., 2011; Sanchez Goñi et al., 2016; Oliveira et al., 2018) and the Asian monsoon (eg. Cheng et al., 2016). Numerous climate model simulations have also been used to understand the response of the climate system to the astronomical forcing. For example, Earth system models of intermediate complexity (EMICs), such as CLIMBER (Ganopolski and Calov, 2011) and GENIE (Holden et al., 2011), have been used to perform long transient simulations to study the climate response to varied astronomical parameters, GHG and NH ice sheets over many glacial-interglacial cycles. More complex atmosphere-ocean general circulations models, such as HadCM3 (Singarayer et al., 2011), have been used to perform snapshot experiments to study the response of one or more components of the climate system to changes in insolation. Both proxy and modelling studies show that the climate response to the astronomical forcing depends strongly on regions and on different climatic variables.

On hemisphere scales, evidence from both paleoclimate records and simulations shows that the two hemispheres seem to respond differently to obliquity and precession. As far as sea ice is concerned, Lo et al. (2018) found that the autumn sea ice extent was governed by precession-dominated insolation when the atmospheric CO_2 concentrations ranging from 190 to 260 ppmv during the last 130 ka in the central Okhotsk Sea. Cronin et al. (2013) reconstructed the sea ice extent during the last 600 ka in western Arctic Ocean and found that the sea ice varied mainly at precessional and obliquity frequencies with precession playing a more important role. In the Southern Ocean, Wolff et al. (2006) reconstructed winter sea ice extent using the ssNa flux over the past eight glacial cycles, and found that its variation was dominated by periodicities on time scales of 80-120 ka although the obliquity and precessional components can also be found. For SST, the reconstructed results also show an obvious difference between the NH and SH. Besides the 100 ka periodicity, the SST reconstructions show a clear obliquity signal in both hemispheres, but the precessional signal is much stronger in the NH than in the SH (Martrat et al., 2007; Bard and Rickaby, 2009). Based on snapshot and 10-times accelerated transient simulations, Yin and Berger (2012, 2015) found that in general the NH climate responds more to precession whereas the SH responds more to obliquity, but in-depth analysis on internal processes and feedbacks are still needed. In addition, Timmermann et al. (2014) investigated the response of the SH climate to obliquity and CO_2 using a series of snapshot simulations and a 5-times accelerated transient simulation. They found that the SH westerlies were mainly controlled by the obliquity cycle and the temperature changes in Antarctica were determined by the combined effect of shortwave obliquity forcing, GHG forcing, and meridional heat transport.

In spite of many existing studies, the different response of the climate system to obliquity and precession between the two hemispheres is still not very clear. This is mainly due to: (1) in the geological records, it is not straightforward to distinguish the impact of the astronomical parameters from the other forcings, like GHG and ice sheets, because they can contain the same periodicities; and (2) the numerical simulations, which focus on understanding the response of the climate system to obliquity and precession and especially the differences between the two hemispheres, are still scarce. Thus, there is a need to investigate the response of the different climatic variables to obliquity and precession using long and continuous transient simulations.

Here we focus on understanding the relative importance of precession and obliquity on two important components in the climate system, sea ice and sea surface temperature, in both hemispheres as well as the internal processes and feedbacks involved to explain the differences between the two hemispheres. Our study is based on a transient simulation using the model LOVECLIM (see section 2 for model description). Although LOVECLIM is classified as an Earth system model of intermediate complexity, its complexity is on the top of this kind of models and thus it can not be used easily to run a transient simulation spanning several glacial cycles. Therefore, in our study, we choose the time interval between 511 and 417 ka BP which covers the interglacial peak of MIS-13, the glacial MIS-12 and the beginning of MIS-11. There are three reasons to choose this period. First, this period includes relatively high and low values of eccentricity which leads to both large and small amplitude of variations in precession and therefore in daily insolation. In particular, it covers MIS-11 with near-zero eccentricity that has been considered as an astronomical analogue of our present-day interglacial (Loutre and Berger, 2003). Second, this period includes both situations where precession minima and obliquity maxima are in-phase and are anti-phase (Fig. 1) (the phase relationship between precession and obliquity could be critical for the climate system (Yin and Berger, 2010, 2015)). Third, this period covers the Mid-Brunhes Transition or Event (MBT or MBE) that is characterized by relatively warmer interglacials after about 430 ka BP than before (eg. Jansen et al.,1986; Jouzel et al., 2007). The causes proposed to explain the MBE includes for example astronomical forcing (Pisias and Rea, 1988; Yin, 2013) and a major ice-sheet expansion during MIS-12 (Bard and Rickaby, 2009). In this study, we don't intend to investigate the MBE, but our results and simulation might be useful for other studies working on this topic.

2 Model and experiment design

LOVECLIM is a three dimension Earth system Model of Intermediate Complexity (Goosse et al., 2010). In our study, the atmosphere (ECBilt), the terrestrial biosphere (VECODE), and the ocean and sea ice (CLIO) are interactively coupled. ECBilt is a spectral atmospheric model with truncature T21, which corresponds approximately to a horizontal resolution of 5.625°×5.625°. It has three vertical layers and its dynamics are governed by the quasi-geostrophic potential vorticity. VECODE is a two-dimensional dynamical terrestrial vegetation model including two plant functional types: tree and grass, and its resolution is the same as ECBilt. CLIO is a global free-surface ocean general circulation model coupled to a thermodynamic-dynamic sea ice model. The horizontal resolution of CLIO is 3° in longitude and latitude, and there are 20 unevenly spaced levels along vertical in the ocean. LOVECLIM and its previous versions have been used in many paleoclimate studies ranging from polar climate dynamics to tropical monsoon (see references in Goosse et al., 2010). It is shown that

LOVECLIM reproduces the major characteristics of climate changes for both present-day and some important past periods (Goosse et al., 2010). Its performance over polar regions is particularly demonstrated. For example, it has been shown that LOVECLIM simulates reasonably well the present-day sea ice extent in both hemispheres when compared with the observations, and its results are similar to those of many sophisticated general circulation models in simulating the sea ice changes during the Holocene, the last Glacial Maximum and the last millennium (Goosse et al., 2013). The transient simulations over the last 9000 years using ECBilt-CLIO-VECODE show a good agreement between the simulated long-term sea ice evolution and proxy records in both hemispheres (Renssen et al. 2005a, 2005b).

Our transient simulation is more than 90,000-years long and uses time-dependent astronomical parameters of the period between 511 and 417 ka BP, a time interval corresponding to MIS-13, MIS-12 and the beginning of MIS-11. Covering four precessional cycles and two obliquity ones, it allows to investigate the impact of a large range of precession and obliquity. In order to investigate the impact of insolation alone, only astronomical parameters (Berger, 1978) vary in time. Constant GHG concentrations (CO_2=236 ppmv, CH_4=530 ppbv, N_2O=265 ppbv) are used and the ice sheets are fixed to present-day. In order to avoid any possible influence of the acceleration technique, no acceleration is used in our study. The initial condition of our transient simulation is the equilibrium climate state of a 2000-year snapshot simulation performed with the astronomical parameters at 511 ka BP and the GHG concentrations same as the transient experiment.

It is worth noting that the experiment we carried out is a sensitivity experiment and the GHG concentrations and ice sheets conditions used do not correspond to the real conditions during MIS-13, MIS-12 and MIS-11. The GHG concentrations used here are the average values over 20,000 years between 511 to 491 ka BP, and are intermediate between a typical interglacial level (eg. 280 ppmv) and a glacial level (e.g. 180 ppmv). In order to test the sensitivity of our results to the choice of CO_2 concentration, we performed another two supplementary simulations covering a shorter period between 538 and 471 ka BP. The CO_2 concentration is kept constant to a value of 280 ppmv in one simulation and it varies with time between about 245 and 190 ppmv in another. These simulations show that our conclusion remains the same for a range of CO_2 concentration between 280 and 190 ppmv (see supplementary Fig. S1).

3 Results and discussion

(1) Sea ice

Fig. 1 shows clearly that the responses of the Arctic and Southern Ocean sea ice to the astronomical forcing are different. In the Arctic, the variation of the annual mean sea ice is highly correlated with precession, while in the Southern Ocean, it is highly correlated with obliquity. In order to quantify the relative weight of each astronomical parameter on the sea ice variations, multiple linear regression analyses (using the standardized values of the variables) are performed. The results (Table 1) show that precession plays a dominant role on the Arctic sea ice and the importance of obliquity is also obvious, but obliquity is more important for the Southern Ocean sea ice. Our results on the Arctic sea ice is in line with the finding of Lo et al. (2018) where both proxy records and numerical simulations show that the sea ice in the central Okhotsk sea during the last 130,000 years is mainly governed by precession-dominated insolation changes when the atmospheric CO_2 concentrations ranging from 190 to 260 ppmv. Cronin et al. (2013) also indicate that the sea ice in western Arctic Ocean during the last 600 ka varied primarily at precessional and obliquity frequencies, and precession plays a dominant role. As CO_2 and ice sheets are fixed in our simulation, it is impossible for us to discuss about the 100 ka cycle that might be strongly related to these forcings (Clark et al., 1999). However, the Southern Ocean sea ice reconstruction of Wolff et al. (2006) shows a dominant 80-120 ka cycle. This indicates that other forcings than insolation, such as GHG and ice sheets, must have a major influence on the Southern Ocean sea ice. Indeed, Yin and Berger (2012) show that GHG plays a dominant role in the SH whereas insolation is more important in the NH.

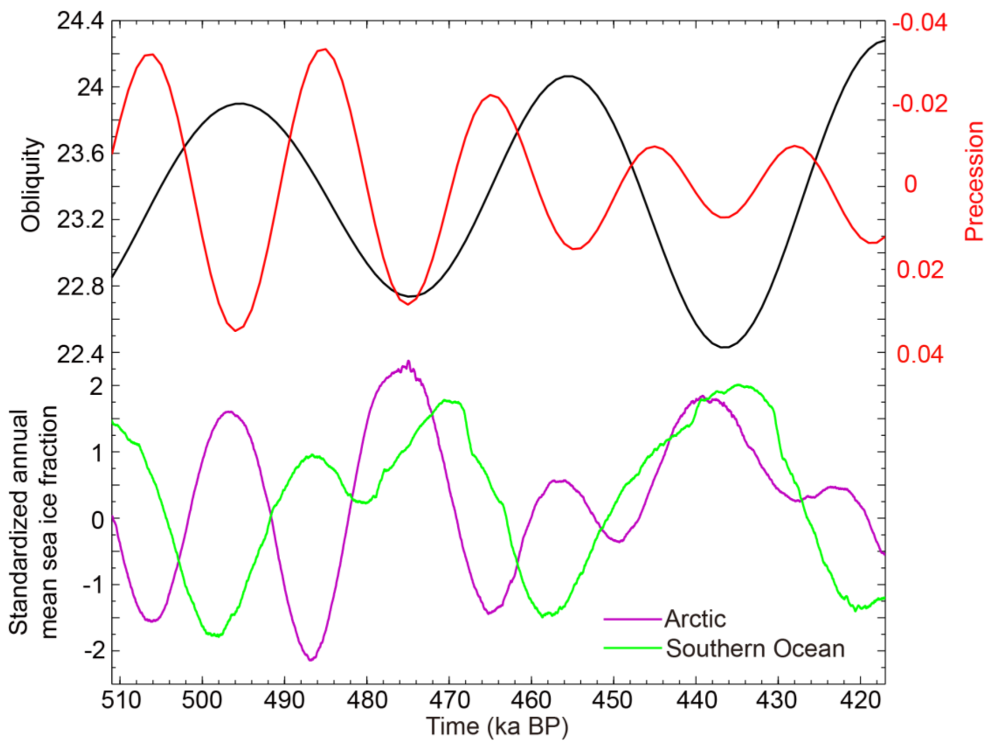

Fig. 1. Comparison of the simulated annual mean Arctic and Southern Ocean sea ice fraction with obliquity and precession. A 1000-year running mean is performed on the curves of the Arctic and Southern Ocean sea ice fraction to reduce the high-frequency fluctuations.

Table 1 Regression coefficients of a linear multiple regression between the insolation-induced climatic variables (the predictand) and E (eccentricity), O (obliquity) and P (precession) (the predictors). The calculation is based on the data of the whole simulation period between 511 and 417 ka BP. The variables are annual mean sea ice fraction and sea surface temperature. All the values have been standardized to have the regression coefficients representing comparable weights of the predictors on the predictand.

	sea ice fraction		sea surface temperature (SST)						
	Arctic	Southern Ocean	60°S-90°S	30°S-60°S	10°S-30°S	10°S-10°N	10°N-30°N	30°N-60°N	60°N-90°N
R^2	0.77	0.67	0.86	0.90	0.40	0.12	0.32	0.68	0.74
E	-0.15	-0.14	0.10	0.11	0.15	0.06	0.05	-0.07	-0.04
O	-0.45	-0.72	0.91	0.93	0.38	-0.16	0.20	0.75	0.65
P	0.78	-0.24	-0.02	-0.19	-0.51	-0.29	-0.55	-0.50	-0.68

Our simulation period contains a period of high amplitude variation of precession (511-460 ka BP) and a period of low amplitude variation of precession (460-417 ka BP). We might expect a dominant role of obliquity when the variation of precession is small, as shown in Yin and Berger (2015) for MIS-11. Therefore, we also performed separately linear multiple regression analyses for 511-460 ka BP and for 460-417 ka BP. The results of 511-460 ka BP are very similar to those obtained from the whole time period (see supplementary Table S1), but the results of 460-417 ka BP (Table S2) show that obliquity is more important than precession in both the Arctic and Southern Ocean sea ice, which is quite expected from the low amplitude variation of precession. However, obliquity still plays more important role in the SH than in the NH and precession is more important in the NH than SH even in the latter case.

To better understand the different response of the Arctic and Southern Ocean sea ice to precession and obliquity, and related internal processes and feedbacks, the seasonal variations of the Arctic and Southern Ocean sea ice are also analyzed (Fig. 2). In the Arctic, the amplitude of the sea ice variation is much larger in summer than in other seasons (Fig. 2a), this is in line with the results of snapshot simulations of the last nine interglacials (Yin and Berger, 2012) and the observation records over the last 30 years (Titchner and Rayner, 2014). This can also be observed by comparing the seasonal geographical distributions of sea ice fraction between a precession maximum (e.g. 496 ka BP) and a precession minimum (e.g. 486 ka BP) (Fig. S2 and Fig. S3). The variation of the annual mean sea ice is therefore dominated by the variation of the summer sea ice, which is mainly controlled by local summer insolation that in turn is mainly a function of precession. When climatic precession is low (NH summer at perihelion), the local summer insolation is high, leading to low sea ice fraction (Fig. 3, left). In addition, the Arctic sea ice is also influenced, but to a lesser degree, by the northward oceanic heat transports across 60°N (Goosse and Renssen, 2001) which is also dominated by precession (not shown). However, the local summer insolation also contains obvious obliquity signal, a smaller obliquity directly leading to lower summer insolation and finally to a cooling and more sea ice formation, which could explain why obliquity is also present in the Arctic sea ice (Table 1). In the Southern Ocean, the difference in the magnitude of sea ice variations between the four seasons is smaller than in the Arctic, but the amplitude is still the largest in local summer (Fig. 2, Fig. S2 and Fig. S3). The annual mean sea ice variation is more equally influenced by the variations of the sea ice of the four seasons when compared to Arctic. Different from the summer sea ice variation in the Arctic, the variation of the summer sea ice in the Southern Ocean shows a very strong obliquity signal. These explain why obliquity is more important for the sea ice in the Southern Ocean than in the Arctic. A smaller obliquity directly leads to lower insolation at high latitudes and finally to a cooling and more sea ice formation (Fig. 3, right), and vice versa. In addition, obliquity could also influence the Southern Ocean sea ice through its influence on the westerlies. Our results (Fig. 3, right) show that a smaller obliquity leads to larger latitudinal temperature and pressure gradients, and finally to stronger westerly winds. In line with Timmermann et al. (2014), in our simulation the SH westerlies are mainly influenced by obliquity. According to some sensitivity experiments performed by other studies, stronger westerlies could cool the ocean surface and lead to more sea ice formation (Purich et al., 2016; Saunders et al, 2018). Therefore, a smaller obliquity could lead to more sea ice formation in the Southern Ocean through decreasing local solar radiation and intensifying the westerlies. The formation of the Southern Ocean sea ice may also be influenced by the southward oceanic heat transports across 60°S that is dominated by precession (not shown). This might partly explain why there is a weak precessional signal in the annual mean Southern Ocean sea ice (Table 1). This agrees with the geological evidence that the Southern Ocean sea ice variation also contains precession periodicity (Wolff et al., 2006).

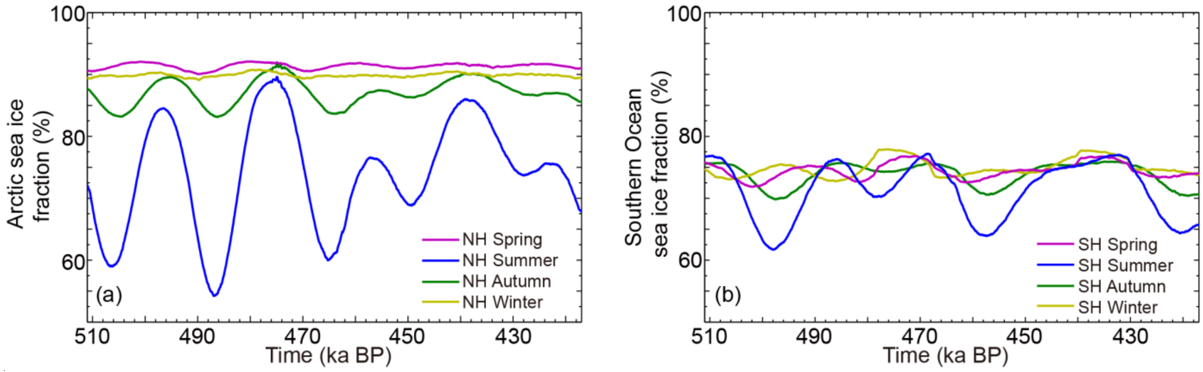

Fig. 2. The seasonal variations of the sea ice fraction in the (a) Arctic and (b) Southern Ocean. A 1000-year running mean is performed on the curves to reduce the high-frequency fluctuations.

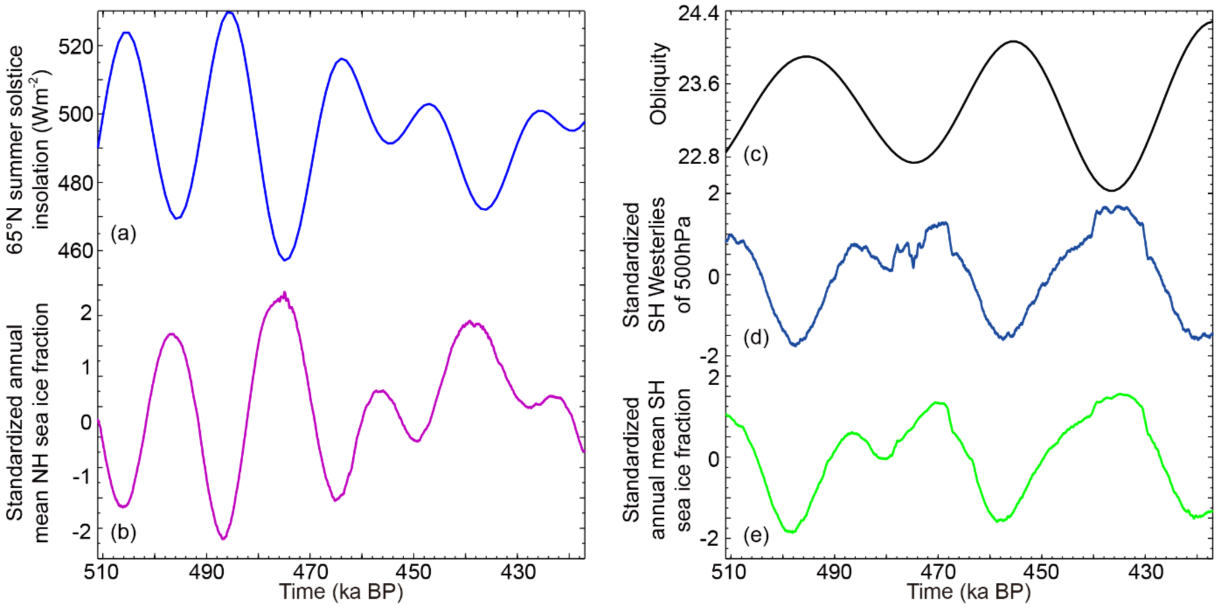

Fig. 3. The forcing mechanisms for the annual mean Arctic (left) and Southern Ocean sea ice (right). (a) 65°N summer solstice insolation, (b) standardized annual mean Arctic sea ice

fraction, (c) obliquity, (d) standardized SH westerlies of 500hPa, (e) standardized annual mean Southern Ocean sea ice fraction. A 1000-year running mean is performed on the curves of (b), (d), and (e) to reduce the high-frequency fluctuations.

The key internal processes responsible for the response of sea ice to precession and obliquity lie in the relationships between the surface energy budget (surface solar radiation – surface thermal radiation + surface sensible heat flux + surface latent heat flux), SST and sea ice. Fig. 4 shows that the surface energy budget (40°N-90°N and 40°S-90°S) is directly related to the SST (40°N-90°N and 40°S-90°S) which in turn influence the sea ice: when the surface energy budget is high, SST is high, leading finally to less sea ice, for a relationship which happens in both hemispheres (but the sea ice could also influence the SST, a feedback which will be discussed below). The surface energy budget is directly and strongly influenced by precession and obliquity: linear multiple regression analyses (Table 2) show that obliquity plays a dominant role in the SH surface energy budget whereas precession is more important in the NH, explaining the different response of the NH and SH sea ice to precession and obliquity. The different response of the annual mean sea ice between the Arctic and Southern Oceans to obliquity and precession is related to their different geographic locations. The Arctic is located in the northern highest polar latitudes, while the Southern Ocean is located between about 60°S and 75°S; so the amplitude of the local summer insolation variation is much larger in the Arctic than in the Southern Ocean. In addition, the large area of the SH ocean makes it reacting more slowly than lands surrounding the Arctic Ocean and therefor more sensitive to the total energy integrated over time that is only a function of obliquity (Berger and Pestiaux, 1984; Berger et al., 2010). If the two periods 511-460 ka BP and 460-417 ka BP are considered separately, the results of the surface energy budget are in line with those of sea ice, the importance of obliquity being enhanced during 460-417 ka BP due to the low amplitude variation of precession (Table S3 and Table S4).

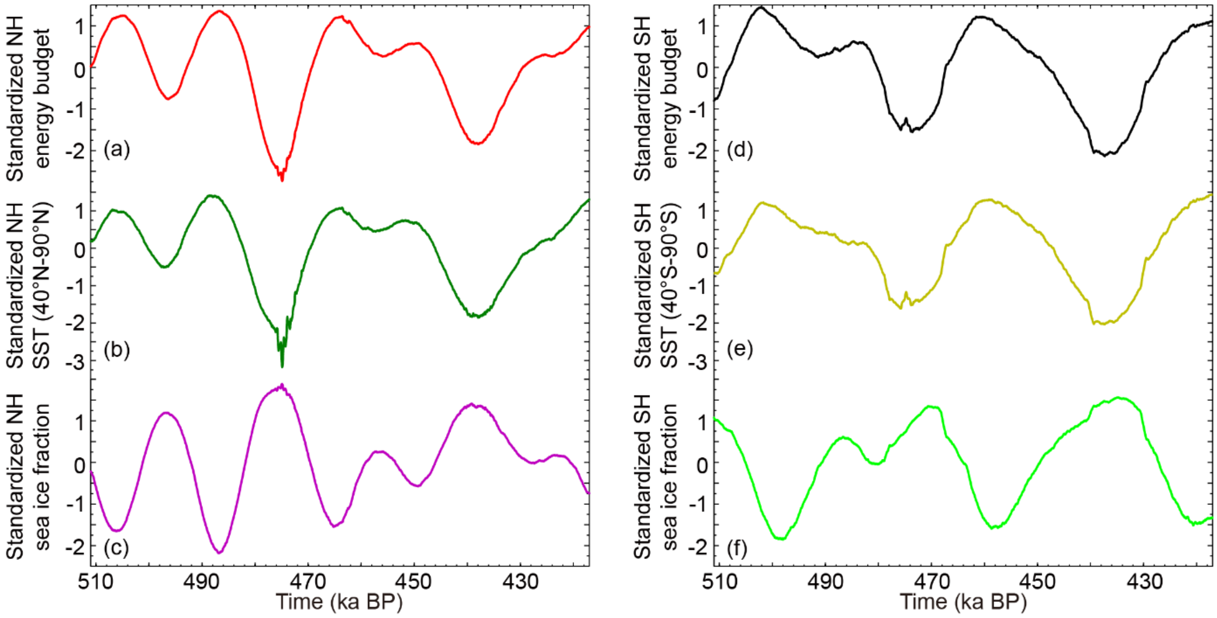

Fig. 4. Comparison of the standardized annual mean sea ice fraction with the standardized annual mean SST and surface energy budget. (a) surface energy budget in the NH (40°N-90°N), (b) SST in the NH (40°N-90°N), (c) Arctic sea ice fraction, (d) surface energy budget in the SH (40°S-90°S), (e) SST in the SH (40°S-90°S), (f) Southern Ocean sea ice fraction. A 1000-year running mean is performed on the curves to reduce the high-frequency fluctuations.

Table 2 Regression coefficients of a linear multiple regression between the surface energy budget (the predictand) and E (eccentricity), O (obliquity) and P (precession) (the predictors). The calculation is based on the data of the whole simulation period between 511 and 417 ka BP. The surface energy budget has been standardized to have the regression coefficients representing comparable weights of the predictors on the predictand.

	surface energy budget			
	40°N-90°N	40°S-90°S	60°N-90°N	60°S-90°S
R^2	0.91	0.84	0.87	0.83
E	0.04	0.18	0.01	0.10
O	0.70	0.86	0.69	0.90
P	-0.75	-0.28	-0.74	-0.18

(2) SST at different latitudinal bands

The SST variations at the low latitudes of both NH and SH show strong precessional signals (Fig. 5), which can be partly explained by the very strong precessional signal in the daily insolation at low latitudes (Berger, 1978). In addition, the oceanic heat transports have a great contribution to the variations of the SST at low latitudes of both hemispheres, as shown from modern reanalysis data (Trenberth and Caron, 2001). Our simulated oceanic heat transports at low latitudes show very strong precessional signals (not shown), which could also explain the strong precessional signal in our simulated SST at low latitudes.

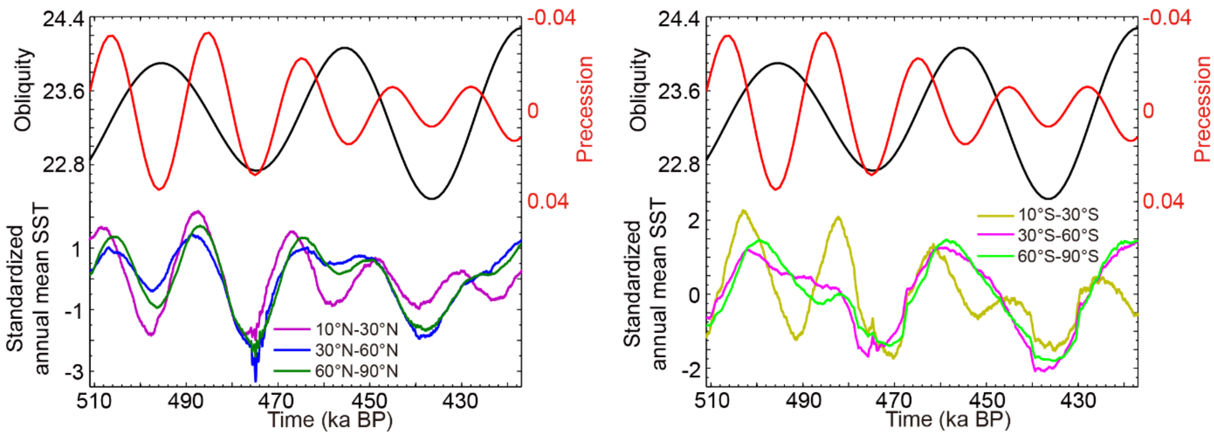

Fig. 5. Comparison of the simulated standardized annual mean SST in the NH (left) and SH (right) with obliquity and precession. A 1000-year running mean is performed on the curves of the SST to reduce the high-frequency fluctuations.

At mid and high latitudes, there are obvious differences between the NH and SH in the SST response. In the SH, the SST variations are highly correlated with obliquity, while they are highly correlated with both obliquity and precession in the NH (Fig. 5 and Table 1). In terms of proxy data, almost all SST records show strong periodicity around 100 ka after the mid-Pleistocene transitions. This is not shown in our simulated SST, most probably because only insolation is used in our experiment as forcing, GHG and ice sheets being kept constant.

Besides the 100 ka cycle signals, in geological record, the SST of both hemispheres shows strong obliquity signal, but the precessional signal is much stronger in the NH than in the SH (Martrat et al., 2007; Bard and Rickaby, 2009). This is consistent with our simulated results. Compared to low latitudes, obliquity has a larger effect on the daily insolation at mid and high latitudes (Berger, 1978). Thus, the SST variations at mid and high latitudes of both hemispheres show stronger obliquity signals. In the meantime, the different distribution of continents and oceans between the NH and SH lead to different response in the two hemispheres. Due to the relatively slow response of oceans, the SST variations in the SH, where large area of oceans appear, are more sensitive to integrated insolation which is only a function of obliquity (Berger and Pestiaux, 1984; Berger et al., 2010). In the NH, the precessional forcing can be amplified by vegetation dynamics, leading to strong precessional signal in the annual mean SST variations (Claussen et al., 2006; Ganopolski and Roche, 2010). In a previous study where LOVECLIM was used to study the last nine interglacials, it was also shown that the vegetation change in the NH mid and high latitudes is mainly controlled by precession (Yin and Berger, 2012). The same is found in our study for the time period investigated and the simulated vegetation shows strong precession signal (not shown). In addition, the variation of the Arctic sea ice shows strong precessional signal while the variation of the Southern Ocean sea ice shows strong obliquity signal, which would also influence the SST variations through sea ice-temperature feedbacks. Both vegetation and sea ice feedbacks in the NH explain the strong precessional signals in the NH SST variations. As discussed above, the key internal processes responsible for the response of SST to precession and obliquity are related to surface energy budget. Our results show that the surface energy budget and SST have a very good and positive relationship (for instance, at high latitudes of both hemispheres, Fig. 6). When the surface energy budget is high, the SST is also high, and vice versa. Obviously, the surface energy budget is highly correlated with obliquity in the SH, while it is highly correlated with both precession and obliquity in the NH (Fig. 6 and Table 2), which could explain the different response of the NH and SH SST at mid and high latitudes to precession and obliquity. The different response of the surface energy budget to precession and obliquity between two hemispheres is also due to the different distribution of continents and oceans in the NH and SH as discussed above.

If we analyze the results of 511-460 ka BP and 460-417 ka BP separately (Table S1 and Table S2), the results of 511-460 ka BP are similar to those obtained from the whole time period, but precession signal is more amplified as expected from the high amplitude variation of precession during this time period. It is also as expected from the low amplitude variation of precession during 460-417 ka BP, obliquity plays a more important role than precession in the SST in both NH and SH mid and high latitudes during this time period. Nevertheless, precession is still more important in the NH than SH, similar to the results of sea ice. The results of the multiple linear regression analyses for the surface energy budget are consistent with the SST (Table S3 and Table S4).

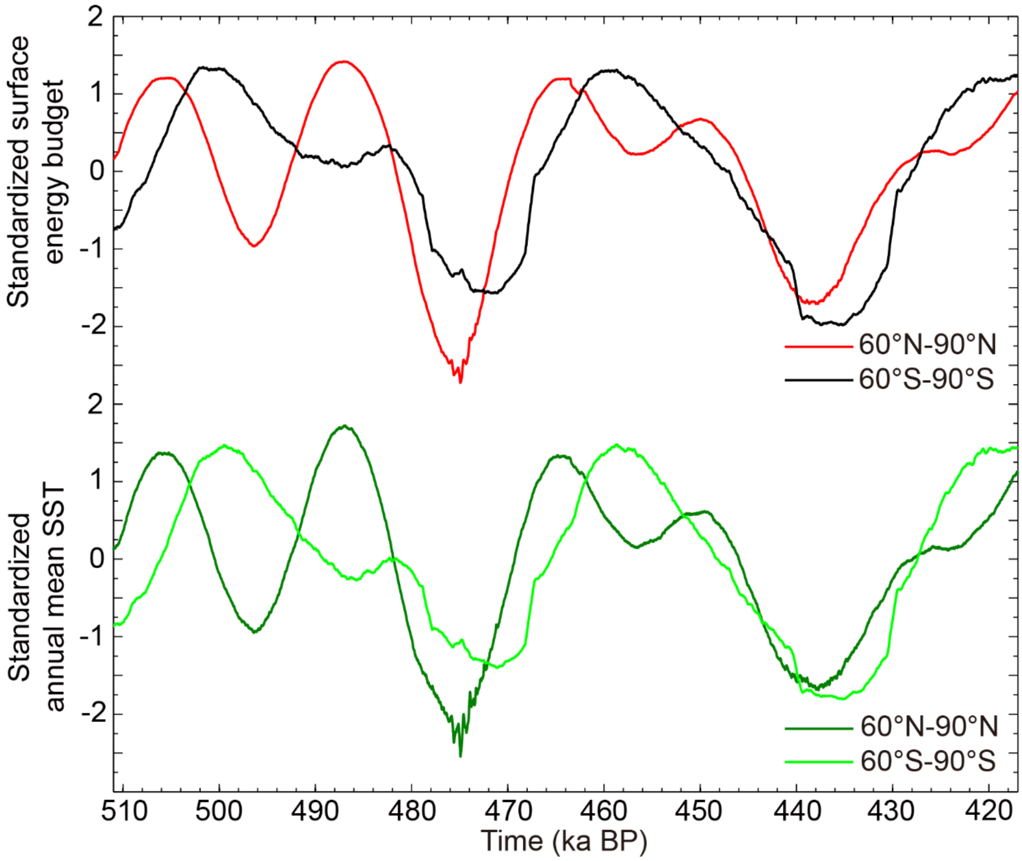

Fig. 6. Comparison between the standardized annual mean SST at high latitudes and the standardized annual mean surface energy budget. A 1000-year running mean is performed on the curves to reduce the high-frequency fluctuations.

(3) SST near the Equator

The annual mean SST near the Equator (10°S-10°N) shows very intriguing variation (Fig. 7). Like the SST at low latitudes, the SST near the Equator shows strong precessional signal, but it also contains strong half-precessional signal (Fig. 7 and Fig. 8). Obviously, the half-precessional signal is the strongest between 511 ka BP and 460 ka BP, but it is less obvious between 460 ka BP and 417k aBP most probably due to the small amplitude variation of precession which dampens the half-precessional signal.

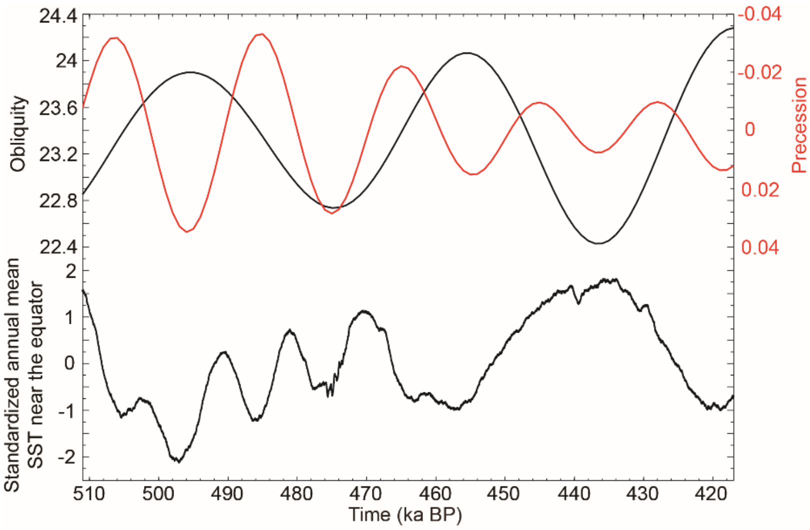

Fig. 7. The variation of the annual mean SST near the equator. A 1000-year running mean is performed on the curves of the SST to reduce the high-frequency fluctuations.

To better understand the half-precessional signal in the SST near the Equator, the SST time series were pre-whitened by subtracting 20% weighted averages using Kaleidagraph software (Cleveland, 1979) (20% = windows/the total time series*100%). This removal of long-term trends helps to emphasizes the half-precessional signal from the strong precessional signal. After subtracting 20% weighted averages, the detrended SST variation (Fig. 8a, grey line) was analyzed by using the multi-taper method (MTM) spectral estimator (Thomson, 1982), and the spectra shows significant peak at ~10 kyr with the significance at above the 99% confidence level (Fig. 8b). In order to discuss the possible forcing mechanism for the half-precessional cycle in the SST near the Equator, Gaussian band pass filtering was applied by using Analyseries 2.0.8 (Paillard et al., 1996) to extract the half-precessional signal (Fig. 8a, blue line), and it has a good coherence with the original data (Fig. 8a, grey line).

The half-precessional signal has already been found in different geological records, like marine sediments (Luo et al., 2005; Ferretti et al., 2010, 2015), vegetation (Turney et al., 2004), lake sediments (Chaisson et al., 2002; Trauth et al., 2003), loess (Sun and Huang, 2006), and ice cores (Delmotte et al., 2004; Guo et al., 2012). In addition, some possible forcing mechanisms have also been proposed by Berger et al. (2006) to explain it. In the inter-tropics, the Sun goes ahead twice a year at each latitude. Especially, the Sun culminates at the zenith at both equinoxes at the Equator. Thus, the inter-tropical regions can receive twice maximum insolation during one year. During one precession cycle, maximum insolation at these regions can be recorded twice. Therefore, if the proxies are sensitive to maximum insolation, the half-precession cycle signal can be recorded (Berger et al., 2006; Ashkenazy and Gildor, 2008). In our study, the half-precessional signal in the SST near the Equator is particularly strong and consistent with the maximum equatorial insolation (Fig. 8c). This shows that in our simulation, the half-precessional signal is clearly a response to the maximum insolation at the Equator (Berger et al., 2006).

According to some paleoclimate records, half-precession cycle occurs in climate variations not only in the tropics but also in extra-tropics. For example, Hernández-Almeida et al. (2012) suggest that the half-precession signal could be transported from the tropics to high latitudes through atmosphere and ocean circulations and could also be produced through ice sheet feedbacks. It could also be produced by the interactions between the NH and SH. As the NH and SH are 180° out of phase with respect to precession-controlled insolation, the half-precession signal could be produced when the SH signal export to the NH (Rutherford and D'Hondt, 2000; Guo et al., 2012). Furthermore, a series of nonlinear processes of the climate system could also produce the half-precessional signal (Hyde and Crowley, 2002). Different from some proxy records that show half-precessional signal also in the high latitudes (eg. Delmotte et al., 2004), the half-precessional signal is not clear in extra-tropics in our simulation. This is probably due to the lack in our experiment of some internal feedbacks like those related to ice sheet dynamics and/or the simplified physics of our atmosphere model. It would be interesting to test with more sophisticated Earth system models in the future.

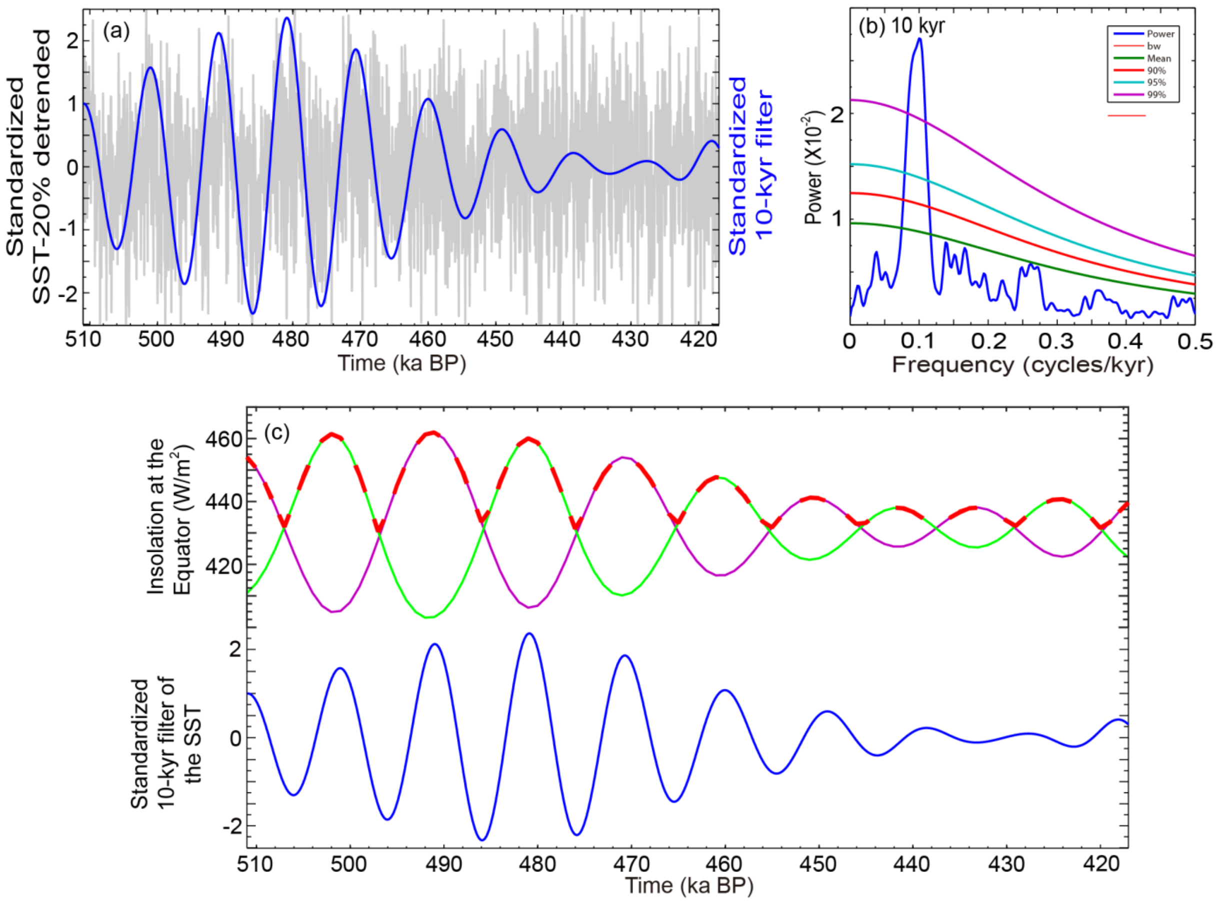

Fig. 8. Analysis of the annual mean SST near the equator. (a) standardized 20% detrended SST (grey line) and standardized 10-kyr filter, (b) power spectra of the 20% detrended SST, (c) comparison between the standardized 10-kyr filter of the SST and the maximum insolation at the equator. The purple line is March-April insolation (one month average), the green line is September-October insolation (one month average), the red dashed line is the maximum of them, and the blue line is the standardized 10-kyr filter of the SST.

4 Conclusions

In this study, the different responses of the SST and sea ice to precession and obliquity between the two hemispheres are investigated through a transient simulation with the LOVECLIM model.

Our results show that the responses are different between the two hemispheres. The Arctic sea ice is highly correlated with precession, while the Southern Ocean sea ice is highly correlated with obliquity. In the Arctic, the variation of the annual mean sea ice is dominated by the variation in local summer which, through the surface energy budget and SST, is controlled by local summer insolation that in turn is mainly a function of precession. It is also influenced by the northward oceanic heat transports across 60°N which is mainly controlled by precession. In the Southern Ocean, the sea ice variations are more equally weighted between seasons with the amplitude being slightly larger in local summer during which the sea ice variation is dominated by obliquity. The large area of the SH oceans makes it reacting more slowly and being more sensitive to total energy integrated over time that is only a function of obliquity.

At low latitudes of both two hemispheres, the SST variations show strong precessional signal, due to strong precessional signal in the daily insolation at the low latitudes and also in the oceanic heat transports. Compared with low latitudes, the SST variations at mid-high latitudes show stronger obliquity signal in both two hemispheres due to the increased importance of obliquity in the daily insolation at mid-high latitudes. Due to sea ice and vegetation feedbacks and also large continental area, the SST variations in the mid-high latitudes of the NH show stronger precessional signal and weaker obliquity signal than in the SH.

Near the Equator, besides the precessional signal, the SST variation in our simulation also shows strong half-precessional signal. The half-precession filter of the SST is highly correlated with the maximum insolation at the Equator, indicating that it is a response to the maximum insolation at the Equator. The lack of half-precessional signal in the SST of other latitudes in our simulation might be due to lack of some internal feedbacks (eg. ice sheet dynamics) and/or simplified atmosphere physics in our model. It would be interesting to be tested with a more complex model.

Our results also show that during the period of low eccentricity and therefore of low amplitude variation of precession, obliquity always plays the dominant role in both sea ice and SST, which is quite expected, but precession is still more important in the NH than in the SH. Half-precessional signal vanishes during low-eccentricity period due to the reduced impact of precession.

Acknowledgments

This work is supported by the Fonds de la Recherche Scientifique-FNRS (F.R.S.-FNRS) under grant MIS F.4529.18 and the National Natural Science Foundation of China (Grant Nos. 41690114 and 41888101). Q.Z. Yin is Research Associate F.R.S.-FNRS. Z.P. Wu thanks Dr. Feng Shi and Rui Zhang for discussion. We also thank the anonymous reviewers for their constructive comments. Computational resources have been provided by the supercomputing facilities of the Université catholique de Louvain (CISM/UCL) and the Consortium des Équipements de Calcul Intensif en Fédération Wallonie Bruxelles (CÉCI) funded by the Fond de la Recherche Scientifique de Belgique (F.R.S.-FNRS) under convention 2.5020.11.

References

Ashkenazy, Y., Gildor, H., 2008. Timing and significance of maximum and minimum equatorial insolation. Paleoceanography 23(1), PA1206. https://doi.org/10.1029/2007PA001436

Bard, E., Rickaby, R. E., 2009. Migration of the subtropical front as a modulator of glacial climate. Nature 460(7253), 380-384. https://doi.org/10.1038/nature08189

Berger, A. L., 1976. Obliquity and precession for the last 5000000 years. Astron. Astrophy. 51, 127-135.

Berger, A. L., 1978. Long-term variations of daily insolation and Quaternary climatic changes. J. Atmos. Sci. 35(12), 2362-2367. https://doi.org/10.1175/15200469(1978)035<2362:LTVODI>2.0.CO;2

Berger, A., Pestiaux, P., 1984. Accuracy and stability of the Quaternary terrestrial insolation, In Milankovitch and climate: understanding the response to astronomical forcing (p.83).

Berger, A., 1988. Milankovitch theory and climate. Rev. Geophys. 26(4), 624-657. https://doi.org/10.1029/RG026i004p00624

Berger, A., Loutre, M. F., Mélice, J. L., 2006. Equatorial insolation: from precession harmonics to eccentricity frequencies. Clim. Past. 2(2), 131-136. https://doi.org/10.5194/cp-2-131-2006

Berger, A., Loutre, M. F., Yin, Q. Z., 2010. Total irradiation during any time interval of the year using elliptic integrals. Quat. Sci. Rev. 29(17-18), 1968-1982. https://doi.org/10.1016/j.quascirev.2010.05.007

Chaisson, W. P., Poli, M. S., Thunell, R. C., 2002. Gulf stream and western boundary undercurrent variations during MIS 10–12 at site 1056, Blake-Bahama Outer Ridge. Mar. Geol. 189(1-2), 79-105. https://doi.org/10.1016/S0025-3227(02)00324-9

Cheng, H., Edwards, R. L., Sinha, A., Spötl, C., Yi, L., Chen, S. T., Kelly, M., Kathayat, G., Wang, X. F., Li, X. L., Kong, X. G., Wang, Y. J., Ning, Y. F., Zhang, H. W., 2016. The Asian monsoon over the past 640,000 years and ice age terminations. Nature 534(7609), 640-646. doi:10.1038/nature18591

Clark, P. U., Alley, R. B., Pollard, D., 1999. Northern Hemisphere Ice-Sheet Influences on Global Climate Change. Science 286, 1104-1111.

Claussen, M., Fohlmeister, J., Ganopolski, A., Brovkin, V., 2006. Vegetation dynamics amplifies precessional forcing. Geophys. Res. Lett. 33, L09709. https://doi.org/10.1029/2006GL026111

Cleveland, W. S., 1979. Robust locally weighted regression and smoothing scatterplots. J. Am. Stat. Assoc. 74(368), 829-836. doi:10.1080/01621459.1979.10481038

Cronin, T. M., Polyak, L., Reed, D., Kandiano, E. S., Marzen, R. E., Council, E. A., 2013. A 600-ka Arctic sea-ice record from Mendeleev Ridge based on ostracodes. Quat. Sci. Rev. 79, 157-167. https://doi.org/10.1016/j.quascirev.2012.12.010

de Garidel-Thoron, T., Rosenthal, Y., Bassinot, F., Beaufort, L., 2005. Stable sea surface temperatures in the western Pacific warm pool over the past 1.75 million years. Nature 433(7023), 294-298. doi:10.1038/nature03189

Delmotte, M., Chappellaz, J., Brook, E., Yiou, P., Barnola, J. M., Goujon, C., Raynaud, D., Lipenkov, V. I., 2004. Atmospheric methane during the last four glacial‐interglacial cycles: Rapid changes and their link with Antarctic temperature. J. Geophys. Res.-Atmos. 109(D12). https://doi.org/10.1029/2003JD004417

Ferretti, P., Crowhurst, S. J., Hall, M. A., Cacho, I., 2010. North Atlantic millennial-scale climate variability 910 to 790 ka and the role of the equatorial insolation forcing. Earth Planet. Sci. Lett. 293(1-2), 28-41. https://doi.org/10.1016/j.epsl.2010.02.016

Ferretti, P., Crowhurst, S. J., Naafs, B. D. A., Barbante, C., 2015. The Marine Isotope Stage 19 in the mid-latitude North Atlantic Ocean: astronomical signature and intra-interglacial variability. Quat. Sci. Rev. 108, 95-110. https://doi.org/10.1016/j.quascirev.2014.10.024

Ganopolski, A., Roche, D. M., 2010. On the nature of lead-lag relationships during glacial-interglacial climate transitions. Quat. Sci. Rev. 28(27-28), 3361-3378. https://doi.org/10.1016/j.quascirev.2009.09.019

Ganopolski, A., Roche, D. M., 2011. 100 kyr World: the role of carbon dioxide, regolith and eolian dust. Clim. Past. 7, 1415-1425. doi:10.5194/cp-7-1415-2011

Goosse, H., Renssen, H., 2001. A two-phase response of the Southern Ocean to an increase in greenhouse gas concentrations. Geophys. Res. Lett. 28(18), 3469-3472. https://doi.org/10.1029/2001GL013525

Goosse, H., Brovkin, V., Fichefet, T., Haarsma, R., Huybrechts, P., Jongma, J., Mouchet, A., Selten, F., . Barriat, P.-Y., Campin, J.-M., Deleersnijder, E., Driesschaert, E., Goelzer, H., Janssens, I., Loutre, M.-F., Morales Maqueda, M. A., Opsteegh, T., Mathieu, P.-P., Munhoven, G., Pettersson, E. J., Renssen, H., Roche, D. M., Schaeffer, M., Tartinville, B., Timmermann, A., Weber, S. L., 2010. Description of the Earth system model of intermediate complexity LOVECLIM version 1.2. Geosci. Model Dev. 3, 603-633. doi:10.5194/gmd-3-603-2010

Goosse, H., Roche, D. M., Mairesse, A., Berger, M., 2013. Modelling past sea ice changes. Quat. Sci. Rev. 79, 191-206. doi:10.1016/j.quascirev.2013.03.011

Guo, Z. T., Zhou, X., Wu, H. B., 2012. Glacial-interglacial water cycle, global monsoon and atmospheric methane changes. Clim. Dyn. 39(5), 1073-1092. https://doi.org/10.1007/s00382-011-1147-5

Hay, J. D., Imbrie, J., Shackleton, N. J., 1976. Variations in the Earth's orbit: pacemaker of the ice ages. Science 194, 1121-1132. doi:10.1126/science.194.4270.1121

Hernández-Almeida, I., Sierro, F. J., Cacho, I., Flores, J. A., 2012. Impact of suborbital climate change in the North Atlantic on ice sheet dynamics at the Mid-Pleistocene Transition. Paleoceanography 27, PA3214. doi:10.1029/2011pa002209

Holden, P. B., Edwards, N. R., Wolff, E. W., Valdes, P. J., Singarayer, J. S., 2011. The Mid-Brunhes Event and West Antarctic ice sheet stability. J. Quat. Sci. 26(5), 474-477. doi:10.1002/jqs.1525

Howard, W. R., Prell, W. L., 1992. Late Quaternary surface circulation of the southern Indian Ocean and its relationship to orbital variations. Paleoceanography 7(1), 79-117. https://doi.org/10.1029/91PA02994

Hyde, W. T., Crowley, T. J., 2002. Stochastic forcing of Pleistocene ice sheets: Implications for the origin of millennial-scale climate oscillations. Paleoceanography 17(4), 1-8. https://doi.org/10.1029/2001PA000669

Jansen, J. H. F., Kuijpers, A., Troelstra, S. R. A., 1986. Mid-Brunhes climatic event: long-term changes in global atmosphere and ocean circulation. Science 232, 619–622. doi:10.1126/science.232.4750.619

Joannin, S., Bassinot, F., Nebout, N. C., Peyron, O., Beaudouin, C., 2011. Vegetation response to obliquity and precession forcing during the Mid-Pleistocene Transition in Western Mediterranean region (ODP site 976). Quat. Sci. Rev. 30(3-4), 280-297. https://doi.org/10.1016/j.quascirev.2010.11.009

Jouzel, J., Masson-Delmotte, V., Cattani, O., Dreyfus, G., Falourd, S., Hoffmann, G., Minster, B., Nouet, J., Barnola, J. M., Chappellaz, J., Fischer, H., Gallet, J. C., Johnsen, S., Leuenberger, M., Loulergue, L., Luethi, D., Oerter, H., Parrenin, F., Raisbeck, G., Raynaud, D., Schilt, A., Schwander, J., Selmo, E., Souchez, R., Spahni, R., Stauffer, B., Steffensen, J. P., Stenni, B., Stocker, T. F., Tison, J. L., Werner, M., Wolff, E. W., 2007.

Orbital and millennial antarctic climate variability over the past 800,000 years. Science 317(5839), 793-796. doi:10.1126/science.1141038

Lawrence, K. T., Herbert, T. D., Brown, C. M., Raymo, M. E., Haywood, A. M., 2009. High-amplitude variations in North Atlantic sea surface temperature during the early Pliocene warm period. Paleoceanography 24(2), PA2212. https://doi.org/10.1029/2008PA001669

Luo, Y., Sun, X., Jian, Z., 2005. Environmental change during the penultimate glacial cycle: a high-resolution pollen record from ODP Site 1144, South China Sea. Mar. Micropaleontol. 54(1-2), 107-123. https://doi.org/10.1016/j.marmicro.2004.09.006

Loutre, M. F., Berger, A., 2003. Marine isotope stage 11 as an analogue for the present interglacial. Glob. Planet. Chang. 36(3), 209-217. https://doi.org/10.1016/S0921-8181(02)00186-8

Loutre, M. F., Paillard, D., Vimeux, F., Cortijo, E., 2004. Does mean annual insolation have the potential to change the climate?. Earth Planet. Sci. Lett. 221(1-4), 1-14. https://doi.org/10.1016/S0012-821X(04)00108-6

Lo, L., Belt, S. T., Lattaud, J., Friedrich, T., Zeeden, C., Schouten, S., Smik, L., Timmermann, A., Cabedo-Sanz, P., Huang, J-J., Zhou, L. P., Ou, T-H., Chang, Y-P., Wang, L-C., Chou, Y-M., Shen, C-C., Chen, M-T., Wei, K-Y., Song, S-R., Fang, T-H., Gorbarenko, S. A., Wang, W-L., Lee, T-Q., Elderfield, H., Hodell, D. A., 2018. Precession and atmospheric CO_2 modulated variability of sea ice in the central Okhotsk Sea since 130,000 years ago. Earth Planet. Sci. Lett. 488, 36-45. https://doi.org/10.1016/j.epsl.2018.02.005

Martrat, B., Grimalt, J. O., Shackleton, N. J., de Abreu, L., Hutterli, M. A., Stocker, T. F., 2007. Four climate cycles of recurring deep and surface water destabilizations on the Iberian margin. Science 317(5837), 502-507. doi:10.1126/science.1139994

Oliveira, D., Desprat, S., Yin, Q. Z., Naughton, F., Trigo, R., Rodrigues, T., Abrantes, F., Goñi, M. F. S., 2018. Unraveling the forcings controlling the vegetation and climate of the best orbital analogues for the present interglacial in SW Europe. Clim. Dyn. 51(1-2), 667-686. doi:10.1007/s00382-017-3948-7

Paillard, D., Labeyrie, L., Yiou, P., 1996. Macintosh program performs time-series analysis. Eos, Transactions AGU 77(39), 379-379. https://doi.org/10.1029/96EO00259

Pisias, N. G., Rea, D. K., 1988. Late pleistocene paleoclimatology of the central equatorial pacific: sea surface response to the southeast trade winds. Paleoceanography 3(1), 21-37. doi:10.1029/pa003i001p00021

Purich, A., Cai, W., England, M. H., Cowan, T., 2016. Evidence for link between modelled trends in Antarctic sea ice and underestimated westerly wind changes. Nat. Commun. 7, 10409. https://doi.org/10.1038/ncomms10409

Renssen, H., Goosse, H., Fichefet, T., Brovkin, V., Driesschaert, E., Wolk, F., 2005a. Simulating the Holocene climate evolution at northern high latitudes using a coupled atmosphere-sea ice-ocean-vegetation model. Clim. Dyn. 24, 23-43. doi:10.1007/s00382-004-0485-y

Renssen, H., Goosse, H., Fichefet, T., Masson-Delmotte, V., Koç, N., 2005b. Holocene climate evolution in the high-latitude Southern Hemisphere simulated by a coupled atmosphere-sea ice-ocean-vegetation model. Holocene 15(7), 951-964. doi:10.1191/0959683605hl869ra

Rutherford, S., D'Hondt, S., 2000. Early onset and tropical forcing of 100,000-year Pleistocene glacial cycles. Nature 408(6808), 72-75. https://doi.org/10.1038/35040533

Sanchez Goñi, M. F., Rodrigues, T., Hodell, D. A., Polanco-Martinez, J. M., Alonso-Garcia, M., Hernandez-Almeida, I., Desprat, S., Ferreti, P., 2016. Tropically-driven climate shifts in southwestern Europe during MIS 19, a low eccentricity interglacial. Earth Planet. Sci. Lett. 448, 81-93. doi:10.1016/j.epsl.2016.05.018

Saunders, K. M., Roberts, S. J., Perren, B., Butz, C., Sime, L., Davies, S., Nieuwenhuyze, W. V., Grosjean, M., Hodgson, D. A., 2018. Holocene dynamics of the Southern Hemisphere westerly winds and possible links to CO_2 outgassing. Nat. Geosci. 11, 650-655. https://doi.org/10.1038/s41561-018-0186-5

Singarayer, J. S., Valdes, P. J., Friedlingstein, P., Nelson, S., Beerling, D. J., 2011. Late holocene methane rise caused by orbitally controlled increase in tropical sources. Nature 470(7332), 82-85. doi:10.1038/nature09739

Sun, J. M., Huang, X.G., 2006. Half-precessional cycles recorded in Chinese loess: response to low-latitude insolation forcing during the Last Interglaciation. Quat. Sci. Rev. 25(9-10), 1065-1072. https://doi.org/10.1016/j.quascirev.2005.08.004

Thomson, D. J., 1982. Spectrum estimation and harmonic analysis. Proc. IEEE 70(9), 1055-1096.

Timmermann, A., Friedrich, T., Timm, O. E., Chikamoto, M. O., Abe-Ouchi, A., Ganopolski, A., 2014. Modeling obliquity and CO_2 effects on Southern Hemisphere climate during the past 408ka. J. Clim. 27(5), 1863-1875. https://doi.org/10.1175/JCLI-D-13-00311.1

Titchner, H. A., Rayner, N, A., 2014. The Met Office Hadley Centre sea ice and sea surface temperature data set, version 2: 1. Sea ice concentrations. J. Geophys. Res.-Atmos. 119(6), 2864-2889. https://doi.org/10.1002/2013JD020316

Trauth, M. H., Deino, A. L., Bergner, A. G., Strecker, M. R., 2003. East African climate change and orbital forcing during the last 175 kyr BP. Earth Planet. Sci. Lett. 206(3-4), 297-313. https://doi.org/10.1016/S0012-821X(02)01105-6

Trenberth, K. E., Caron, J. M., 2001. Estimates of meridional atmosphere and ocean heat transports. J. Clim. 14(16), 3433-3443. https://doi.org/10.1175/1520-0442(2001)014<3433:EOMAAO>2.0.CO;2

Turney, C. S., Kershaw, A. P., Clemens, S. C., Branch, N., Moss, P. T., Fifield, L. K., 2004. Millennial and orbital variations of El Nino/Southern Oscillation and high-latitude climate in the last glacial period. Nature 428(6980), 306. https://doi.org/10.1038/nature02386

Wolff, E. W., Fischer, H., Fundel, F., Ruth, U., Twarloh, B., Littot, G. C., Mulvaney, R., Röthlisberger, R., de Angelis, M., Boutron, C. F., Hansson, M., Jonsell, U., Hutterli, M. A., Lambert, F., Kaufmann, P., Stauffer, B., Stocker, T. F., Steffensen, J. P., Bigler, M., Sigggaard-Andersen, M. L., Udisti, R., Becagli, S., Castellano, E., Severi, M., Wagenbach, D., Barbante, C., Gabrielli, P., Gaspari, V., 2006. Southern Ocean sea-ice extent, productivity and iron flux over the past eight glacial cycles. Nature 440(7083), 491-496. https://doi.org/10.1038/nature04614

Yin, Q. Z., Berger, A., 2010. Insolation and CO2 contribution to the interglacial climate before and after the Mid-Brunhes Event. Nat. Geosci. 3(4), 243-246. doi:10.1038/ngeo771

Yin, Q. Z., Berger, A., 2012. Individual contribution of insolation and CO_2 to the interglacial climates of the past 800,000 years. Clim. Dyn. 38(3-4), 709-724. https://doi.org/10.1007/s00382-011-1013-5

Yin, Q. Z., 2013. Insolation-induced mid-Brunhes transition in Southern Ocean ventilation and deep-ocean temperature. Nature 494(7436), 222-225. doi:10.1038/nature11790

Yin, Q. Z., Berger, A., 2015. Interglacial analogues of the Holocene and its natural near future, Quat. Sci. Rev. 120, 28-46. https://doi.org/10.1016/j.quascirev.2015.04.008

SUPPLEMENTARY INFORMATION

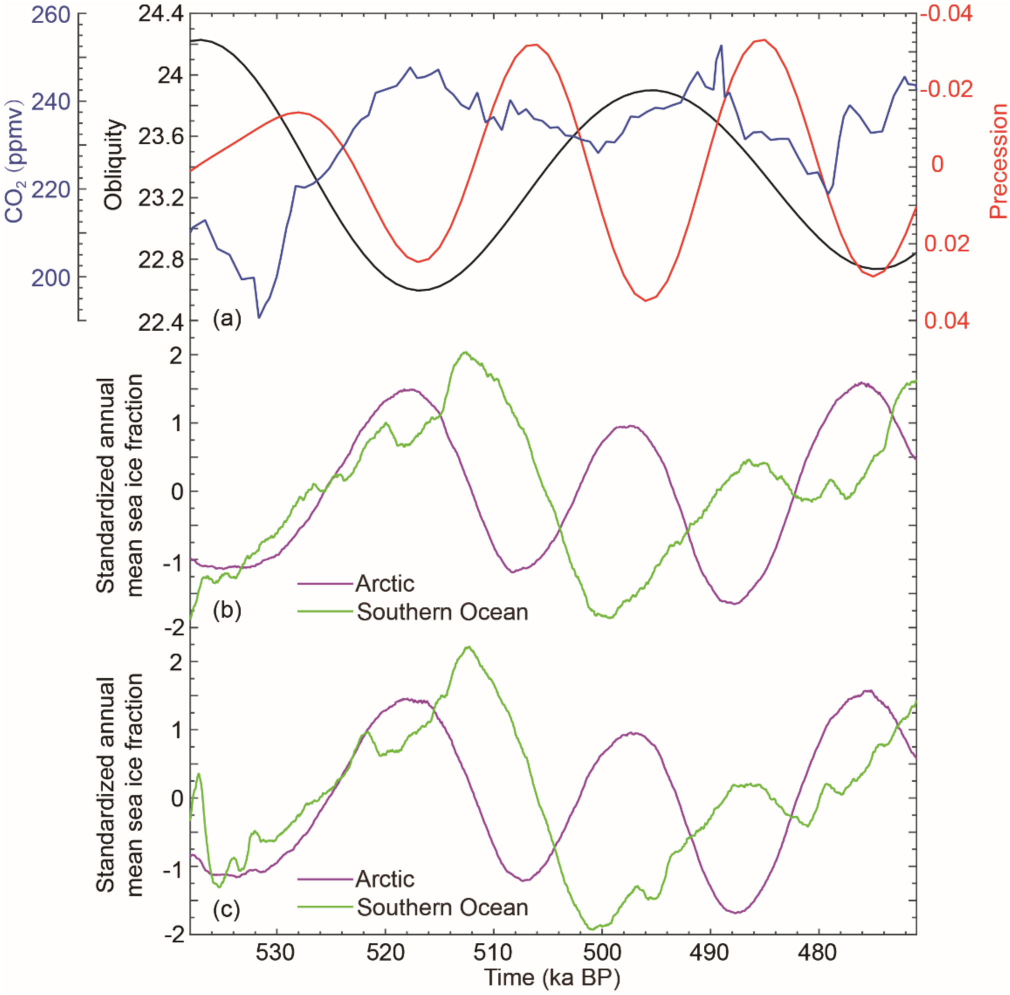

Fig. S1. The simulated variations of the Arctic and Southern Ocean sea ice fraction. (a) the variations of the forcings: CO_2 (blue line), obliquity (black line) and precession (red line), (b) The variations of the Arctic and Southern Ocean sea ice fraction simulated with varying insolation and a constant CO_2 concentration of 280 ppmv, (c) The variations of the Arctic and Southern Ocean sea ice fraction simulated with varying insolation and varying CO_2 as shown in (a).

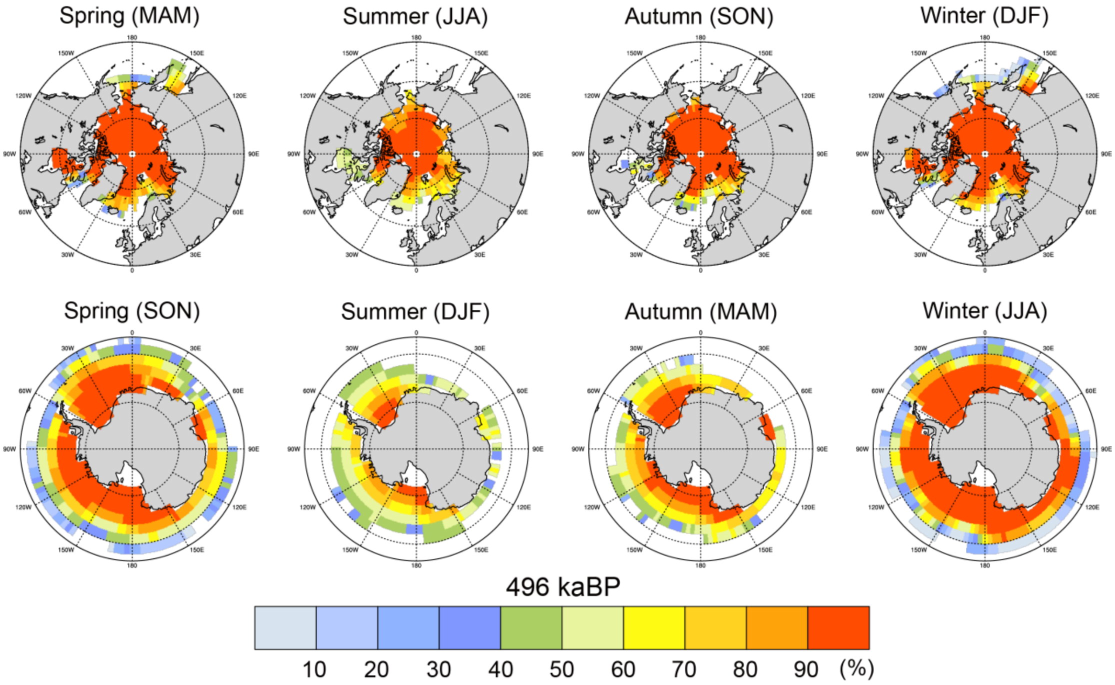

Fig. S2. The seasonal (local seasons are used) geographical distribution of the Arctic and Southern Ocean sea ice at a precession maximum (496 ka BP).

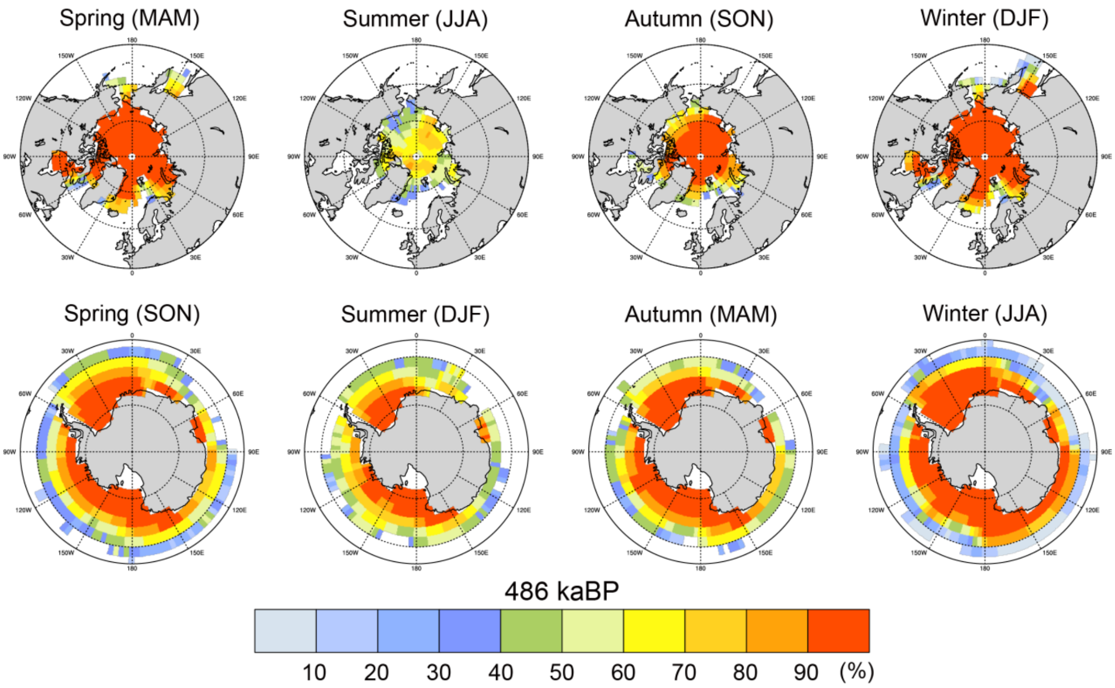

Fig. S3. The seasonal (local seasons are used) geographical distribution of the Arctic and Southern Ocean sea ice at a precession minimum (486 ka BP).

Table S1 Regression coefficients of a linear multiple regression between the insolation-induced climatic variables (the predictand) and E (eccentricity), O (obliquity) and P (precession) (the predictors). The calculation is based on the data of the simulation period between 511 and 460 ka BP. The variables are annual mean sea ice fraction and sea surface temperature. All the values have been standardized to have the regression coefficients representing comparable weights of the predictors on the predictand.

	sea ice fraction		sea surface temperature (SST)						
	Arctic	Southern Ocean	60°S-90°S	30°S-60°S	10°S-30°S	10°S-10°N	10°N-30°N	30°N-60°N	60°N-90°N
R^2	0.81	0.49	0.71	0.87	0.39	0.17	0.44	0.51	0.79
E	-0.04	-0.06	0.07	0.13	0.26	-0.12	0.08	0.08	0.04
O	-0.24	-0.62	0.83	0.87	0.41	-0.33	0.01	0.44	0.34
P	0.88	-0.28	-0.05	-0.33	-0.44	-0.17	-0.68	-0.57	-0.84

Table S2 Regression coefficients of a linear multiple regression between the insolation-induced climatic variables (the predictand) and E (eccentricity), O (obliquity) and P (precession) (the predictors). The calculation is based on the data of the simulation period between 460 and 417 ka BP. The variables are annual mean sea ice fraction and sea surface temperature. All the values have been standardized to have the regression coefficients representing comparable weights of the predictors on the predictand.

	sea ice fraction		sea surface temperature (SST)						
	Arctic	Southern Ocean	60°S-90°S	30°S-60°S	10°S-30°S	10°S-10°N	10°N-30°N	30°N-60°N	60°N-90°N
R^2	0.63	0.70	0.93	0.94	0.24	0.28	0.13	0.72	0.65
E	-0.10	-0.30	0.22	0.16	0.01	-0.71	-0.59	0.14	0.01
O	-0.61	-0.98	0.79	0.88	0.53	-0.14	0.65	0.73	0.72
P	0.33	-0.13	-0.05	-0.11	-0.14	0.24	-0.24	-0.32	-0.36

Table S3 Regression coefficients of a linear multiple regression between the surface energy budget (the predictand) and E (eccentricity), O (obliquity) and P (precession) (the predictors). The calculation is based on the data of the simulation period between 511 and 460 ka BP. The surface energy budget has been standardized to have the regression coefficients representing comparable weights of the predictors on the predictand.

	surface energy budget			
	40°N-90°N	40°S-90°S	60°N-90°N	60°S-90°S
R^2	0.90	0.72	0.86	0.66
E	0.07	0.19	0.07	0.11
O	0.43	0.74	0.42	0.78
P	-0.86	-0.39	-0.84	-0.21

Table S4 Regression coefficients of a linear multiple regression between the surface energy budget (the predictand) and E (eccentricity), O (obliquity) and P (precession) (the predictors). The calculation is based on the data of the simulation period between 460 and 417 ka BP. The surface energy budget has been standardized to have the regression coefficients representing comparable weights of the predictors on the predictand.

	surface energy budget			
	40°N-90°N	40°S-90°S	60°N-90°N	60°S-90°S
R^2	0.92	0.89	0.87	0.92
E	-0.02	0.11	-0.14	0.09
O	0.91	0.98	0.95	0.99
P	-0.36	-0.17	-0.32	-0.14

No conflict of interest.